# Loss of the centrosomal protein ALMS1 alters lipid metabolism and the regulation of extracellular matrix-related processes

Brais Bea-Mascato[1,2], Eduardo Gómez-Castañeda[4], Yara E. Sánchez-Corrales[3], Sergi Castellano[3,5], Diana Valverde[*1,2]

[1] CINBIO, Universidad de Vigo, 36310 Vigo, Spain.

[2] Grupo de Investigación en Enfermedades Raras y Medicina Pediátrica, Instituto de Investigación Sanitaria Galicia Sur (IIS Galicia Sur), SERGAS-UVIGO, Vigo, Spain

[3] Genetics and Genomic Medicine Department, Great Ormond Street Institute of Child Health, University College London, London, United Kingdom

[4] Molecular and Cellular Immunology Section, Great Ormond Street Institute of Child Health, University College London, London, United Kingdom

[5] UCL Genomics, Zayed Centre for Research into Rare Disease in Children, University College London, London, United Kingdom

[*]Correspondence: Diana Valverde. Email dianaval@uvigo.es

CINBIO Facultad de Biología, Universidad de Vigo, Campus As Lagoas-Marcosende s/n, 36310 Vigo, Spain

Tel +34 986 811 953

# ABSTRACT

**Background:** Alström syndrome (ALMS) is a rare autosomal recessive disease that is associated with mutations in *ALMS1* gene. The main clinical manifestations of ALMS are retinal dystrophy, obesity, type 2 diabetes mellitus, dilated cardiomyopathy and multi-organ fibrosis, characteristic in kidneys and liver. Depletion of the protein encoded by *ALMS1* has been associated with the alteration of different processes regulated *via* the primary cilium, such as the NOTCH or TGF-β signalling pathways. However, the cellular impact of these deregulated pathways in the absence of ALMS1 remains unknown.

**Methods**: In this study, we integrated RNA-seq and proteomic analysis to determine the gene expression profile of hTERT-BJ-5ta ALMS1 knockout fibroblasts after TGF-β stimulation. In addition, we studied alterations in cross-signalling between the TGF-β pathway and the AKT pathway in this cell line.

**Results:** We found that ALMS1 depletion affects the TGF-β pathway and its cross-signalling with other pathways such as PI3K/AKT, EGFR1 or p53. In addition, alterations associated with ALMS1 depletion clustered around the processes of extracellular matrix regulation and lipid metabolism in both the transcriptome and proteome. By studying the enriched pathways of common genes differentially expressed in the transcriptome and proteome, collagen fibril organisation, β-oxidation of fatty acids and eicosanoid metabolism emerged as key processes altered by the absence of ALMS1. Finally, an overactivation of the AKT pathway was determined in the absence of ALMS1 that could be explained by a decrease in *PTEN* gene expression.

**Conclusion:** ALMS1 deficiency disrupts cross-signalling between the TGF-β pathway and other dependent pathways in hTERT-BJ-5ta cells. Furthermore, altered cross-signalling impacts the regulation of extracellular matrix-related processes and fatty acid metabolism, and leads to over-activation of the AKT pathway.



**Keywords:** ALMS1, TGF-β, AKT, primary cilia, ciliopathy, ECM, lipid metabolism, Alström syndrome.

# INTRODUCTION

Alström syndrome (ALMS, OMIM #203800) is a rare disease caused by mutations in the *ALMS1* gene. The subcellular localisation of the ALMS1 protein in the basal body of the primary cilium, composed of two centrioles, classified ALMS as a ciliopathy (Hearn et al., 2005; Knorz et al., 2010; Jagger et al., 2011; Kobayashi and Dynlacht, 2011). Ciliopathies are a group of diseases on which, the normal function and assembly of the primary cilia is affected. This ciliopathy is clinically characterised by the development of retinal dystrophy, type 2 diabetes mellitus (T2DM), obesity, dilated cardiomyopathy (DCM), hearing loss and multi-organ fibrosis affecting kidneys, liver and lungs (Collin et al., 2002; Zulato et al., 2011; Hearn, 2018).

Primary cilia are sensory organelles formed by microtubules protruding from the cell membrane. They are essential for a variety of physiological and developmental processes such as the control of cell cycle, migration and differentiation (Christensen et al., 2017; Pala et al., 2017; Anvarian et al., 2019). They also play a role in the regulation of various signalling pathways, such as WNT, Sonic Hedgehog (SHh), transforming growth factor β (TGF-β) and other G-protein-coupled receptor-regulated pathways (Ishikawa and Marshall, 2011; May-Simera et al., 2017, 2018; Pala et al., 2017; Anvarian et al., 2019).

The role of the ALMS1 protein is still unclear, with some (Graser et al., 2007; Li et al., 2007; Knorz et al., 2010) but not all (Collin et al., 2005, 2012; Hearn et al., 2005; Chen et al., 2017) studies suggesting a role in ciliogenesis. ALMS1 depletion, however, affects several signalling pathways regulated through primary cilia, such as the NOTCH and TGF-β pathways (Leitch et al., 2014; Álvarez-Satta et al., 2021; Bea-Mascato et al., 2022, 2023). In the NOTCH signalling pathway, ALMS1 depletion leads to the accumulation of receptors in late endosomes. However, it does not affect the recycling of these receptors in the cell line hTERT-RPE1 (Leitch et al., 2014). In the TGF-β pathway, inhibition of *ALMS1* expression lowers phosphorylation/activation of SMAD2 in hTERT-RPE1 (Álvarez-Satta et al., 2021), which could inhibit the canonical TGF-β pathway. Similar results have been described when abolishing other centrosomal proteins. For example, depletion of CEP128 decreases SMAD2 phosphorylation in zebrafish, hTERT-RPE1 and ciliated human

79 foreskin fibroblasts (hFF) after TGF-β activation(Mönnich et al., 2018). However, these
80 alterations were not observed in ALMS1 knockout models in HeLa or hTERT-BJ-5ta (Bea-
81 Mascato et al., 2022). In these models the only alteration detected in the canonical
82 pathway was a slight decrease in SMAD3 phosphorylation/activation in the hTERT-BJ-
83 5ta model (Bea-Mascato et al., 2022). This suggests that alterations in the TGF-β
84 pathway in the absence of ALMS1 may have a greater impact on other signalling
85 pathways that cross-signal with this pathway such as PI3K/AKT or MAPKs (p38, c-JNKs
86 and others) (Finnson et al., 2020).

87 Despite advances in recent years, little is known about the role of ALMS1 in primary cilia
88 and its regulated signalling pathways. Here, we investigate at the RNA and protein level
89 how the absence of ALMS1 expression in hTERT-BJ-5ta affects the TGF-β pathway and
90 other cellular processes.

# 91 MATERIALS AND METHODS

## 92 Cell culture

93 hTERT-BJ-5ta human dermal fibroblasts and HeLa cell lines from American Type Culture
94 Collection (ATCC) were used for this study. A 4:1 composite medium of Dulbecco's
95 minimum essential medium (DMEM, Gibco, Invitrogen, NY, USA) and Medium 199,
96 Earle's Salts (Gibco, Invitrogen, NY, USA), supplemented with 10% fetal bovine serum
97 (FBS) (Gibco, Invitrogen, NY, USA) and 2% penicillin/streptomycin (P/S) (Gibco,
98 Invitrogen, NY, USA) was used to maintain hTERT-BJ-5ta. DMEM medium supplemented
99 with 10% FBS and 2% P/S was used for the HeLa cells. Both cell lines were cultured at
100 37°C with 5% $CO_2$.

## 101 RNA extraction

102 Initially, $3x10^5$ BJ-5ta cells were seeded in 6-well plates by triplicate in DMEM:199
103 10%FBS 2% P/S. After 24h a change of medium was made by adding DMEM:199 2% P/S
104 without FBS and cells were incubated overnight for serum starvation. Next day, TGF-β
105 pathway was stimulated by adding rhTGF-β1 ligand (2ng/mL; R&D Systems; 240-B) for
106 24 hours. Then, the medium was removed, and wells were washed twice with PBS. Cells

107 were harvested in a tube of 1.5 mL after scraping them on PBS. The NYZ total RNA
108 isolation kit (NYZtech, Lisboa, Portugal) was applied following the manufacturing
109 protocol for RNA extraction. Finally, RNA was eluted, and sample concentrations were
110 measured with nanodrop (Thermo Fisher, Waltham, USA).

## 111 RNA-seq and library construction

112 RNA quality control was performed using Bioanalyzer (Agilent, Santa Clara, USA), finding
113 a RIN ≥ 7. Then, RNA enrichment was carried out with the Dynabeads mRNA direct Micro
114 kit (Life Technologies, Carlsbad, USA) following manufacturer's protocol. Sequencing
115 libraries were constructed from cDNA using the Ion Total RNA-seq Kit v2 with ERCC RNA
116 Spike-in Control mix (Thermo Fisher, Waltham, USA). 25µL of each library was
117 sequenced using a PI V2 chip in an Ion Proton Sequencer (Thermo Fisher, Waltham,
118 USA).

119 After sequencing, fastq files were analysed in the Finisterrae II computer cluster of the
120 "Centro de Supercomputación de Galicia" (CESGA). FastQC (http://www
121 .bioinformatics.babraham.ac.uk/projects/fastqc) and MultiQC (Ewels et al., 2016) were
122 used to determine the quality of the samples **(Figure S1 A)**. High-quality reads were
123 aligned with STAR software (Dobin et al., 2013) using the primary assembly of Homo
124 sapiens genome GRCh38.p13 (Gencode v32). We generated a count matrix using the
125 HTSeq software (Anders et al., 2015). Downstream analysis was performed with the
126 following R (version 4.0.5) packages: DESeq2 (Love et al., 2014) to detect differentially
127 expressed genes (DEG; **Figure S1 B-D; Table S1**); and EnrichR (Kuleshov et al., 2016) for
128 enrichment analysis of GO terms and Pathways, collected from different databases
129 (Bioplanet, KEGG, MSigDB and wikipathway) **(Table S3)**. P-values were calculated using
130 Fisher´s exact test and corrected using Benjamini-Hochberg (FDR). Finally, ggplot and
131 pheatmap were used for the visualisation of the results (Wickham, 2016). To validate
132 our homemade DESeq2 pipeline, SARTools (Varet et al., 2016) was applied and the same
133 number of DEG was obtained.

134 The sequences generated in this work have been deposited in NCBI's Gene Expression
135 Omnibus (Barrett et al., 2013) and are accessible through GEO Series accession number
136 GSE209844.

137 ## Protein extraction

138 BJ-5ta cells were seeded at $3x10^5$ in 6-well plates by triplicate in DMEM:199 10%FBS
139 2%P/S. After 24 hours, FBS was removed from the medium and the cells were incubated
140 overnight for serum starvation. The next day, cells were stimulated with rhTGF-β
141 (2ng/mL) for 24 hours. After that, DMEM:199 was removed, and wells were washed
142 twice with PBS. Cells were scrapped in PBS. Then, they were pellet at 10000 rpm for 5
143 min in a Sigma® 1–14 K at 4°C and 100µL of RIPA buffer was added to each sample for
144 cell lysis. Samples were incubated on ice for 10 min in constant agitation. Finally, cell
145 debris was pelleted by centrifugation for 30 min at 12000 rpm and 4 °C. Samples were
146 aliquoted and stored at -80 ºC until the next step of the protocol. Protein quantification
147 was performed by Bradford microplate assay using Bio-Rad protein assay (Bio-rad,
148 Hercules, USA).

149 ## Label-free proteomic profiling

150 Label-free proteomic profiling was performed following the same protocol described in
151 (Bea-Mascato et al., 2022) with the corresponding quality controls **(Figure S2; Table S2)**.
152 Ggplot and pheatmap were used for the results visualisation. Enrichment analysis was
153 performed using the same protocol as described for the transcriptome **(Table S4)**. The
154 mass spectrometry proteomics data of this study have been deposited to the
155 ProteomeXchange Consortium via the PRIDE (Perez-Riverol et al., 2019) partner
156 repository with the dataset identifier PXD035708.

157 ## Networks generation

158 For the generation of the different networks, we used the programme Cytoscape (3.9.0)
159 with Java (11.0.6). For the generation of the enriched route networks, the pipeline
160 described by Reimand et al.(Reimand et al., 2019) was used. Similarity coefficients
161 between nodes (minimum threshold of 0.375) were calculated using the arithmetic
162 mean between the overlap coefficient and the Jaccard index of the different significantly
163 enriched gene sets in the enrichment analysis (FDR < 0.05). After this procedure, the
164 clusters were annotated using the plugins ClusterMaker2, wordCloud and
165 autoanotation. The MCL algorithm was used via the ClusterMaker2 plugin to determine

166 the clusters and then wordCloud and autoannotation were used to annotate the
167 clusters. The settings were maintained to generate the networks of the different
168 datasets.

## 169 p-AKT/AKT activation assays

170 Initially, about $3x10^6$ BJ-5ta control and ALMS1 knockout (KO) cells were plated in
171 100mm dishes (Corning, NY, USA) in DMEM:199 2P/S% without FBS for serum
172 starvation. After 24h of incubation, the rhTGF-β1 ligand was added at a final
173 concentration of 2ng/mL for 0-, 10-, 30-, and 90-min. Dishes were then washed 3 times
174 with PBS and harvested in 1mL of PBS, using a scraper. After that, cells were pelleted by
175 centrifugation in a Sigma® 1–14 K at 4°C, 7,400×g for 10 min and lysed on ice for 10 min
176 using 200 µL of RIPA buffer, containing 1 mM sodium orthovanadate as phosphatase
177 inhibitor (Sigma-Aldrich, Missouri, USA) and 0.1% (v/v) protease inhibitor cocktail
178 (Merck, Darmstadt, Germany). To remove the pellet with cell debris not lysed with RIPA
179 buffer, samples were centrifuged at 4°C, 14,500×g for 30 min, and the supernatant was
180 collected in 1.5mL low binding tubes (Thermo Fisher, Waltham, USA). For protein
181 quantification, the Bio-Rad protein assay reagent was used in a microplate assay. Finally,
182 samples were stored at -80°C until analysis.

## 183 SDS-PAGE, Western blot and quantification

184 Samples were prepared mixing 20µg of protein from each sample with 6.25µL of
185 Laemmli Buffer 4X (Biorad, Hercules, USA), 1.25µL β-mercaptoethanol (BME) and $H_2O_d$
186 up to a final volume of 25µL. After that, samples were boiled at 97ºC for 5 min and run
187 on a 12% Mini-PROTEAN® TGX™ Precast Gel (Biorad, Hercules, USA) for 1 hour at 150V.
188 Proteins were then transferred to a 0.2 µm polyvinylidene fluoride (PVDF) membrane
189 using the Trans-Blot® Turbo™ Transfer System (Biorad, Hercules, USA) following the
190 mixed molecular weight (MW) protocol. Membranes were blocked with in-house TBS-T
191 buffer [TBS/0.1% (v/v) Tween-20] with 5% (w/v) milk for 90min at room temperature
192 (RT). Incubation with the primary antibody was carried out in blocking solution (TBS-T
193 5% milk) overnight at 4°C. For this assay, the following antibodies were used: anti-AKT
194 (1:5000, Abcam, 179463) and anti-p-AKT (1:5000, Abcam, 222489).

195 The next day, the membranes were washed 3 times with PBS. They were then incubated
196 with the secondary antibody in a blocking solution for 1 hour at RT. Goat anti-rabbit IgG
197 H&L (HRP) (Abcam, 205718) was used as a secondary antibody in this assay at 1:5000
198 for p-AKT and 1:10000 for AKT.

199 Finally, Clarity western ECL substrate (Biorad, Hercules, USA) was used to develop the
200 membranes. The photos were taken by exposure on the ChemiDoc system (Biorad,
201 Hercules, USA) after 5 minutes of incubation with the substrate. Quantification of bands
202 was carried on Image Lab software (Biorad, Hercules, USA) using the method of total
203 protein.

## 204 Fluorescent preparations

205 $2x10^4$ HeLa cells (WT and *ALMS1* KO) were seeded in µ-Slide 8-well chambers (IBIDI,
206 Germany). After 24 hours cells were transfected with pcDNA3 GFP-PTEN using
207 Lipofectamine 3000 (Thermo Fisher, Waltham, USA) following the manufacturer's
208 protocol. Cells were incubated overnight at 37°C with 5% $CO_2$. The following day, the
209 medium was changed by adding DMEM 2% P/S and 2%FBS. In addition, rhTGF-β was
210 added to the corresponding wells at a final concentration of 2ng/mL and the plates were
211 incubated again overnight under the same conditions. Finally, on the fourth day, the
212 preparations were marked, fixed and mounted, following the protocol detailed below.

213 200µL of DMEM medium per well containing CellMask (Thermo Fisher, Waltham, USA)
214 at a 1:1000 dilution were added and incubated for 10min at 37°C in the dark. After two
215 washes with PBS, the cells were fixed with 150 µL of 4% paraformaldehyde (PFA) in a
216 1:10 dilution of DMEM medium and incubated for 10min. The PFA diluted in DMEM was
217 removed with 2 washes with PBS and 200 µL of PBS with DAPI was added at a final
218 concentration of 1µg/mL, followed by a 20min incubation in the dark. Finally, the wells
219 were washed 3 times with PBS to remove the DAPI solution and the samples were
220 mounted with 3 drops of Prolong. After incubation for 1 hour at 4°C, the samples were
221 analysed on the Nikon NIE microscope. (Nikon, Tokyo, Japan).

222 This experiment was performed in duplicate on 2 alternate days adding 2 wells in each
223 experiment for each treatment and cell line (WT and KO).

224 GFP-PTEN was a gift from Alonzo Ross (Addgene plasmid # 13039;
225 http://n2t.net/addgene:13039; RRID: Addgene_13039)

## 226 Image acquisition, processing and analysis

227 The images were taken with the Nikon NIE direct microscope at 20X, using the RGB
228 channels for the acquisition of DAPI (Blue), GFP-PTEN with FITC (Green) and CellMask
229 with TRITC (Red). After that, all the images were processed with Fiji (Java 8 version)
230 (Schindelin et al., 2012). The background was subtracted from all images, the resolution
231 was set to 4908x3264 (0.25microns/pixel) and the RGB channels were grouped with the
232 "Merge Channels" option to create the compositions, maintaining the independence of
233 the channels. Cell segmentation was then performed using the biodock platform
234 (https://www.biodock.ai/). Cells were filtered by size to remove any debris that could
235 have been detected as cells by the algorithm. Finally, the signal from the 550 cells with
236 the highest GFP intensity was normalised against the mean of TGF-β stimulated control
237 to obtain the normalised fluorescence values.

## 238 Statistical analysis

239 The proteomic study involved several statistical analyses and data transformations. The
240 data were first normalized using a variance stabilisation procedure (VSN). Data
241 imputation for missing values was carried out using the Minprob approach with a q-
242 value of less than 0.01. Finally, differential expression analysis was performed using the
243 linear protein models of the limma package (Ritchie et al., 2015) included in the DEP R
244 package (Zhang et al., 2018).

245 Transcriptomic normalisation and analysis were performed using DESeq2 (Love et al.,
246 2014). An FDR value < 0.05 was used to determine differentially expressed genes.

247 To analyse statistical differences in the Western blot data, a t-student with a Benjamini,
248 Krieger, & Yekutieli two-stage correlation was used. Finally, the fluorescence imaging
249 results were analysed with a 2-way ANOVA.

250

# RESULTS

## Inhibition of *ALMS1* gene expression causes several alterations of the transcriptome and proteome

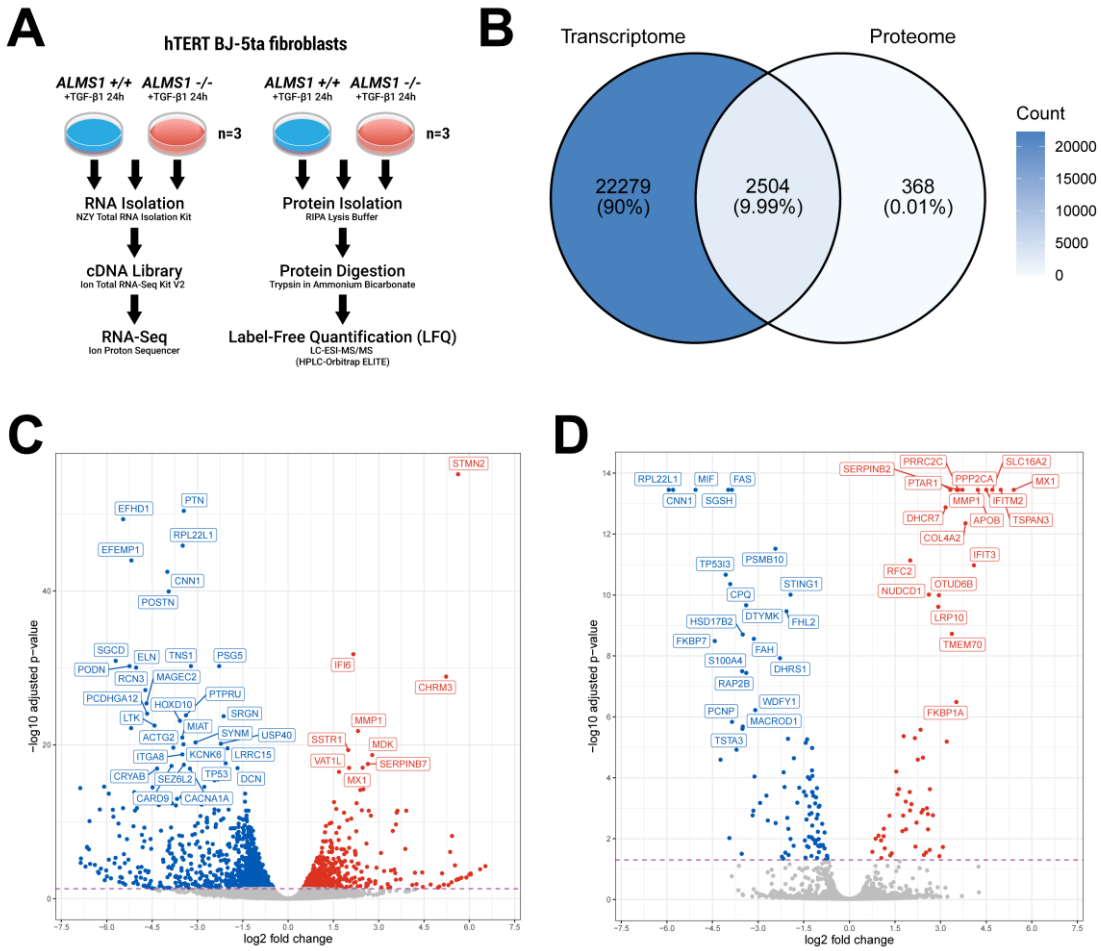


**Figure 1.** Differential expression analysis in the BJ-5ta ALMS1 knockout cell line by RNA-seq and LFQ-proteomics. **(A)** Illustration of the experimental design and procedure followed in this study**.** **(B)** Total overlap between genes identified in the transcriptome and the proteome. **(C)** Volcano-plot of differentially expressed genes (FDR < 0.05) in RNA-seq, highlighting the 40 most significant genes. **(D)** Volcano-plot of differentially expressed proteins (FDR < 0.05) in the proteome, highlighting the 40 most significant protein-coding genes.

In this study, we generated a multi-omics dataset (total RNA-seq and LFQ-proteomic analysis) on an hTERT fibroblast cell line (WT/CT and *ALMS1* KO). This cell line was

263 previously stimulated with TGF-β1 ligand to identify alterations related with TGF-β
264 pathway **(Figure 1A)**.

265 We identified 24,784 genes (transcripts with distinct gene symbols) in the transcriptome
266 **(Figure 1B, Table S1)**. On the other hand, we identified 2,872 proteins in the proteome,
267 of which 1,884 were quantified in the 6 study samples (3WT and 3KO) **(Figure 1B, Figure**
268 **S2A, B, Table S2)**. Of the proteins identified, 2,504 could be unambiguously associated
269 with a gene. These protein-coding genes (PCG) identified in the proteome covered 10%
270 of the total number of genes identified in the transcriptome **(Figure 1B).**

271 Our expression analysis (*ALMS1* KO vs WT) revealed a total of 1,712 differentially
272 expressed genes (DEG) and 158 differentially expressed proteins (DEG) (FDR < 0.05;
273 **Figure 1C, D**). Although the number of DEG detected in the proteome was 10 times
274 lower than in the transcriptome, a similar gene expression profile was observed in both
275 data sets **(Figure 1C, D).** Hence, despite the different resolution of these techniques,
276 they are consistent with each other **(Figure 1B)**.

277

## RNA-seq profiling of *ALMS1*-deficient BJ-5ta cells reveals different pathways related to extracellular matrix regulation

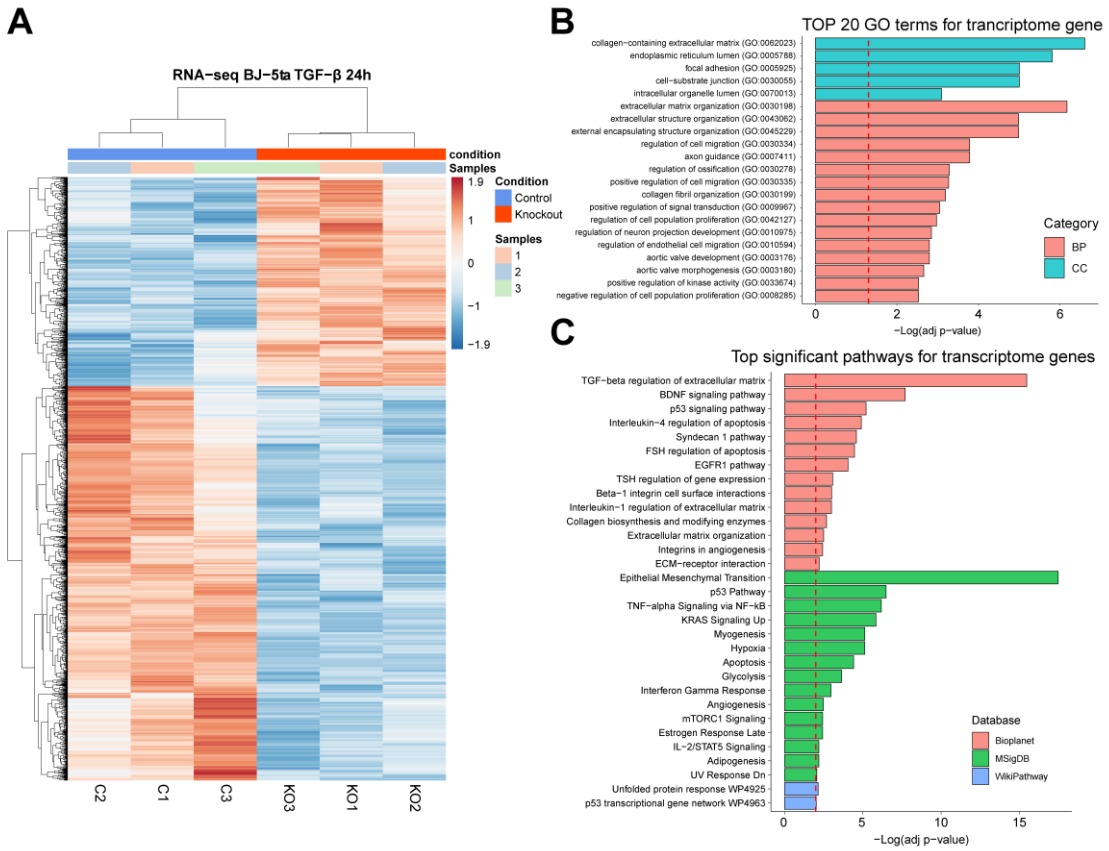


**Figure 2**. RNA-seq expression profile and enrichment analysis in the ALMS1 knockout cell line (hTERT-BJ-5ta). **(A)** Heatmap of the 1,712 differentially expressed genes with FDR < 0.05 in the hTERT-BJ-5ta cell line after 24 hours with TGF-β pathway stimulation **(B)** The 20 most statistically significant GO terms detected after over-representation analysis (ORA) in the transcriptome. BP: biological process; CC: cellular Component **(C)** Signalling pathways significantly enriched (ORA, FDR < 0.01) for trancriptomic data in Bioplanet, KEGG, MSigDB and Wikipathway databases.

In the transcriptome, of 1,712 DEG, 1,119 (65%) were under-expressed and 593 (35%) were over-expressed in the *ALMS1* KO cell line compared to controls **(Figure 2A; Table S1)**.

To determine the processes affected by inhibition of *ALMS1* gene expression in the transcriptome, we performed an over-representation analysis (ORA) **(Table S3)**. DEGs were not filtered by fold change (FC) due to the additive effect of small FCs along a signalling pathway **(Methods)**.

294 We found changes in the gene expression profile of *ALMS1* KO cell line in pathways
295 related to extracellular matrix (ECM) regulation through TGF-β, the Epithelial
296 Mesenchyme Transition (EMT) and various pathways that cross-signal with the TGF-β
297 pathway (BDNF, p53, TNF-α, EGFR1, KRAS and mTORC1) **(Figure 2B, C)**.

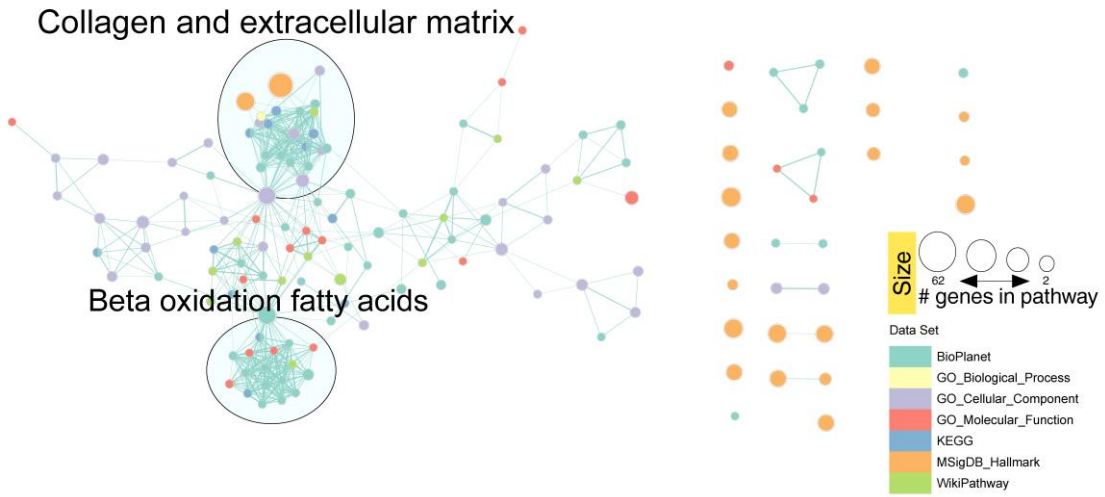


298

299 **Figure 3.** Network clustering of transcriptomic GO terms and enriched routes in the different
300 databases after applying the Markov clustering algorithm (MCL).

301 Next, we constructed a network using EnrichmentMap (Merico et al., 2010) to reduce
302 the redundancy of pathways and processes between the different databases used in the
303 previous analysis. For this, only enrichR terms with an FDR < 0.05 were used **(Methods)**.
304 In this network, we found two main clusters, highly connected to each other,
305 incorporating pathways from different databases. The most representative keywords in
306 these clusters pointed towards collagen and ECM regulation and β-oxidation of fatty
307 acids **(Figure 3)**.

308

309 **Proteomic profiling of *ALMS1*-deficient BJ-5ta cells suggests**
310 **alterations in intracellular organelles lumen and lipid**
311 **metabolism**

312 To study whether the observed differences in gene expression profile are replicated at
313 the protein level, we performed the same analysis on the proteome **(Table S2)**. Of 158
314 DEG, 98 (62%) were under-expressed and 60 (38%) were over-expressed in the *ALMS1*
315 KO cell line **(Figure 4A)**.

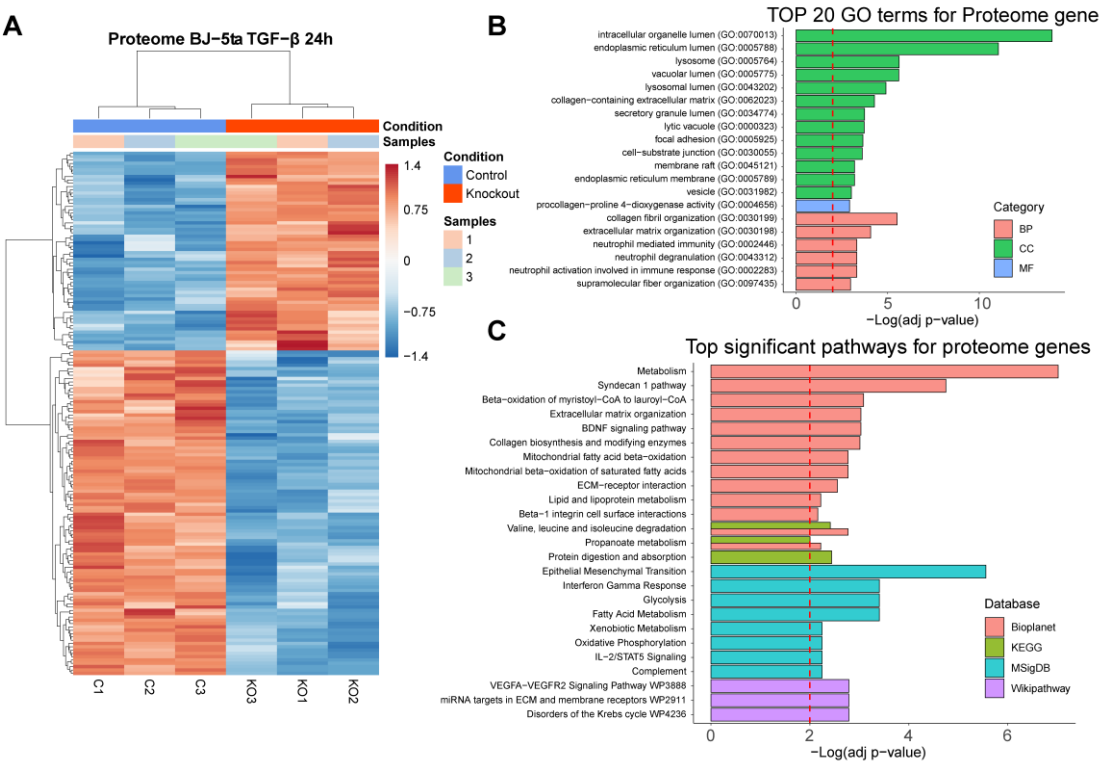


316

317 **Figure 4.** Protein expression profiling and enrichment analysis of ALMS1 knockout cell line
318 (hTERT-BJ-5ta). **(A)** Heatmap of the 158 differentially expressed protein coding genes with FDR
319 < 0.05 in the hTERT-BJ-5ta cell line after 24 hours with TGF-β pathway stimulation **(B)** The 20
320 most statistically significant GO terms detected after over-representation analysis (ORA) in the
321 proteome. BP: biological process; CC: cellular Component; MF: molecular function **(C)** Signalling
322 pathways significantly enriched (ORA, FDR < 0.01) for proteomic data in Bioplanet, KEGG,
323 MSigDB and Wikipathway databases.

324 We performed an ORA to establish the proteome-enriched pathways and GOterms
325 **(Table S4)**. The proteome GO terms suggested that depletion of *ALMS1* gene affects the

326 endoplasmic reticulum, lysosomes, focal adhesion and the organisation of collagen and
327 ECM regulation **(Figure 4B)**. These results are consistent with transcriptome findings,
328 including BDNF, Syndecan-1 signalling pathways and EMT **(Figure 4C)**. In addition, other
329 enriched proteomic pathways involved in metabolic processes such as β-oxidation of
330 fatty acids in mitochondria were also detected **(Figure 4C)**.

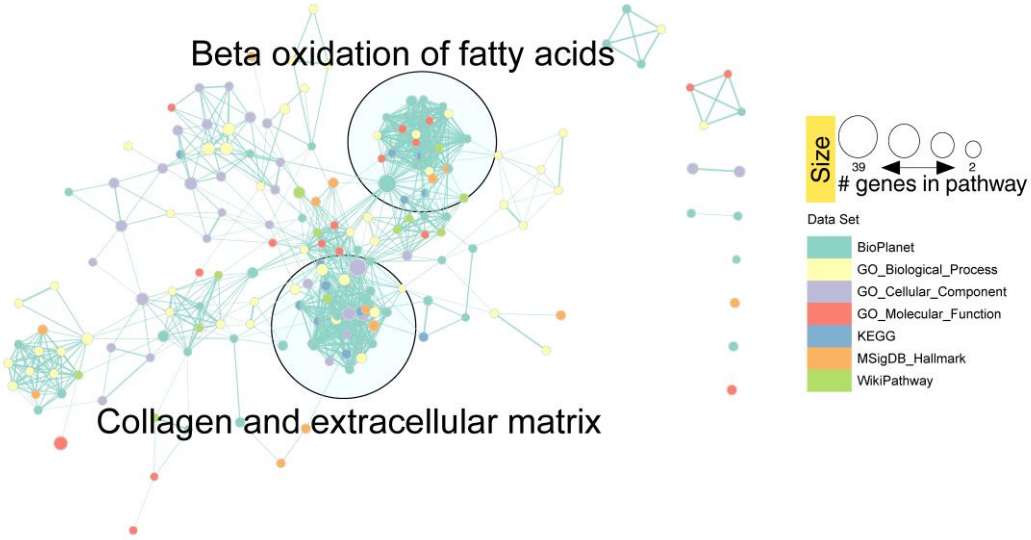


331

332 **Figure 5.** Network clustering of proteomic GO terms and enriched routes in the different
333 databases after applying the Markov clustering algorithm (MCL).

334 Regarding the reduction of redundancy between the databases used for the enrichment
335 analysis, we applied the same methodology as in the previous case, obtaining consistent
336 results with the transcriptome. We found two main clusters, associated with collagen
337 and ECM regulation and β-oxidation of fatty acids **(Figure 5)**.

338

## The multi-omics analysis highlights the association of ALMS1 with the endoplasmic reticulum, Syndecan-1 pathway and EMT

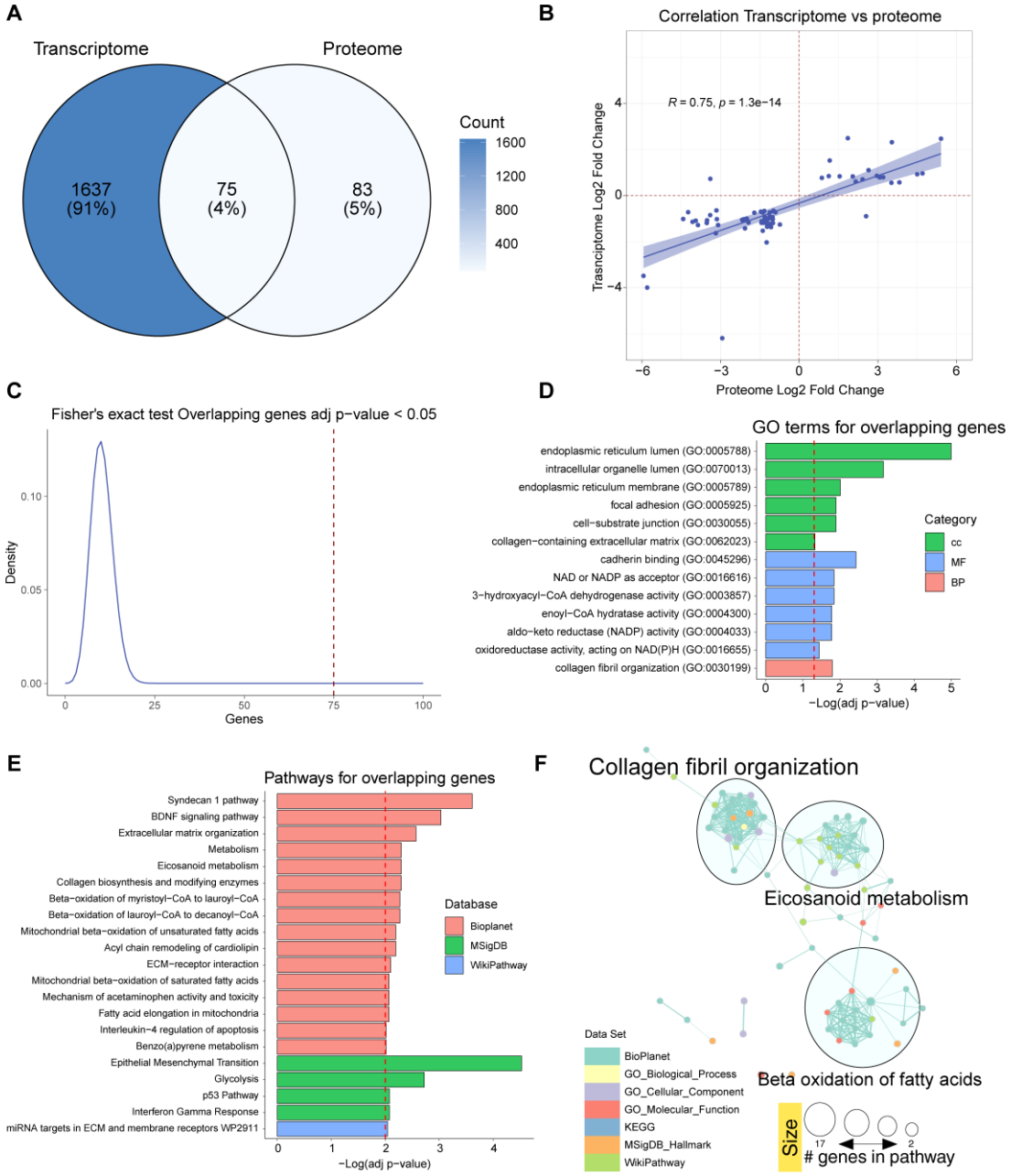


**Figure 6.** Analysis of differentially expressed genes overlapping between transcriptome and proteome. **(A)** Venn diagram with differentially expressed genes in the transcriptome and proteome and matching terms in both datasets. **(B)** Correlation plot between Log2 FCs in the transcriptome and the proteome of the matched terms. **(C)** Fisher's exact test to evaluate the probability of obtaining 75 or more matched genes. **(D)** Significantly over-represented (ORA, FDR < 0.05) GO terms that are associated with the subset of matched data. **(E)** Significantly over-

348 represented pathways (ORA, FDR < 0.01) in the list of overlapping genes **(F)**. Network clustering
349 of GO terms and pathways in the different bases of the overlapping gene data after applying the
350 Markov clustering algorithm (MCL).

351 To investigate the relationship between the transcriptome and proteome, we analysed
352 the overlap of DEG between them (1,712 genes and 158 proteins). This resulted in 75
353 DEG in the *ALMS1* KO cell line **(Figure 6A; Table S5)** with a Pearson correlation of 0.75
354 (p-value $1.3x10^{-14}$) between the FCs of the transcriptome and proteome **(Figure 6B)**.
355 Importantly, the likelihood of finding by chance 75 or more common DEG between the
356 transcriptome and proteome is practically zero (Fisher's exact test). Thus, these genes
357 are a valid signature of ALMS1 depletion **(Figure 6C)**.

358 Further, their enrichment analysis highlights the role of ALMS1 in the endoplasmic
359 reticulum, BDNF or Syndecan 1 pathways, EMT and lipid-associated signalling pathways
360 such as fatty acid metabolism **(Figure 6D, E; Table S6)**. This time, the enriched pathway
361 reduction analysis identified three clusters, one cluster agglutinated the alterations of
362 the ECM, another the alterations of the β-oxidation of fatty acids and the third cluster
363 highlighted the metabolism of eicosanoids, which also affects lipid metabolism **(Figure**
364 **6F)**.

## 365 ALMS1 depletion affects the signalling cross-talk between TGF-β
## 366 and PI3K/AKT

367 ALMS1 depletion does not appear to affect the activation of the canonical TGF-β
368 pathway in all cell types (Bea-Mascato et al., 2022) so the observed alterations could be
369 due to aberrant signalling of non-canonical pathways such as PI3K/AKT. The PI3K/AKT
370 pathway regulates many of the altered processes found in our analyses. This pathway is
371 involved in control of cell migration, proliferation and adhesion (Xu et al., 2015; Yu and
372 Cui, 2016) as well as in cell metabolism (Yu and Cui, 2016; Hoxhaj and Manning, 2019).
373 Given the present results, we decided to study the cross-signalling between the TGF-β
374 and PI3K/AKT pathway in our *ALMS1*-deficient fibroblast line.

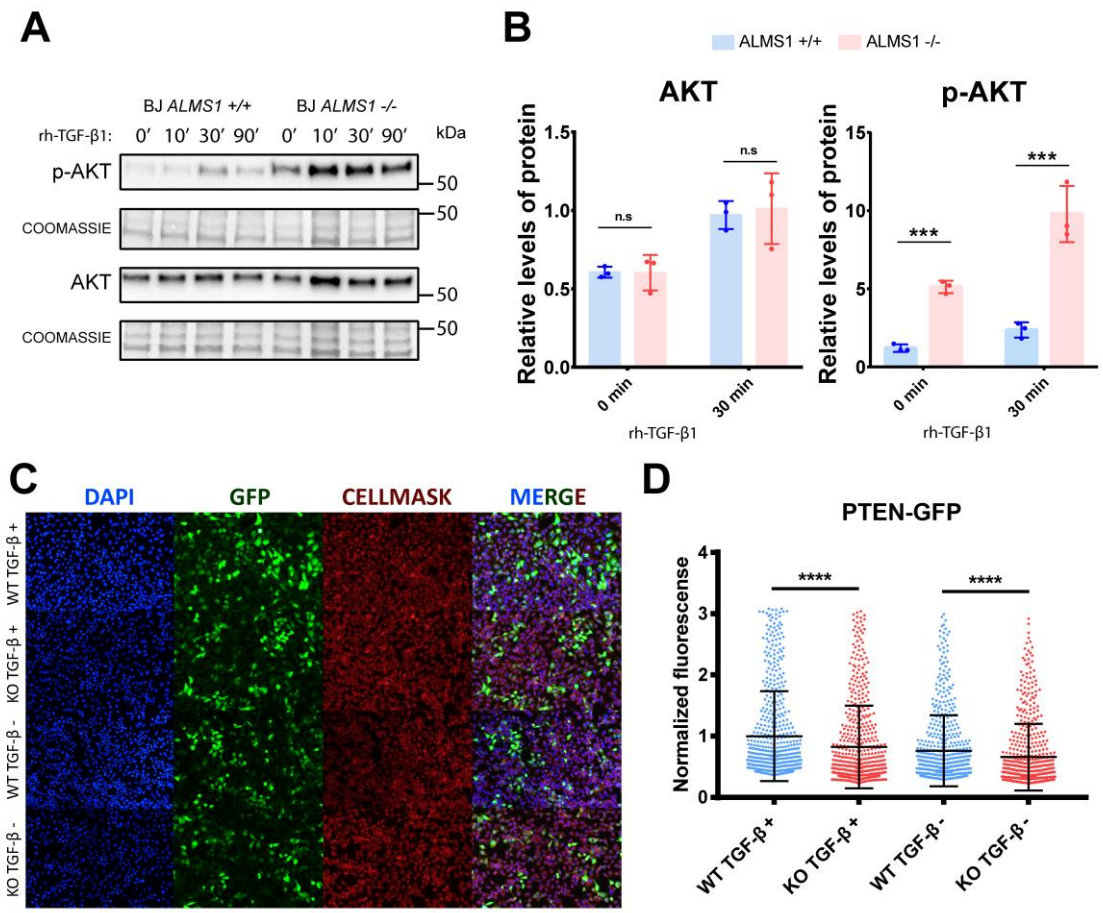


**Figure 7.** Study of cross-signalling between TGF-β and AKT pathways in ALMS1KO cell models. **(A)** Representative Western blot of AKT overactivation after TGF-β pathway stimulation in BJ-5ta. **(B)** Quantification of AKT protein expression and p-AKT activation levels normalised against Coomassie staining in BJ-5ta. **(C)** Representative images of fluorescence labelling of HeLa cells after transfection with GFP-tagged PTEN. **(D)** Normalised fluorescence of the 550 most fluorescent HeLa cells in each preparation.

For this purpose, AKT protein phosphorylation levels were measured in the hTERT-BJ-5ta *ALMS1* KO cell line by Western blot at four different stimulation times with TGF-β1 ligand (0, 10, 30 and 90 min). Indeed, deficiency of *ALMS1* generates an over-activation of the AKT pathway **(Figure 7A, B)**. This over-activation was present at basal level (time 0), but was exacerbated by TGF-β stimulation, with the differentials between ALMS1KO and WT being most notable in AKT after 30min of TGF-β1 stimulation **(Figure 7A, B).**

We thus hypothesised that over-activation of the AKT pathway results from the accumulation of membrane phospholipids such as PIP3, which is the substrate for the

390 activation of PI3K and subsequently AKT. The PTEN protein is responsible for
391 dephosphorylating PIP3 to PIP2 which inhibits the AKT pathway. For this reason, the
392 PTEN inhibition could be a cause of the AKT over-activation. To test this hypothesis, we
393 transfected a KO model for the *ALMS1* gene in the HeLa cell line with a plasmid to
394 express PTEN protein fused to GFP. We observed a significant reduction of GFP
395 fluorescence in the KO cells compared with controls in both untreated and TGF-β ligand-
396 treated cells (p-value < 0.0001). This suggests that ALMS1 depletion affects PTEN
397 expression. Moreover, this inhibition seems to be slightly accentuated (p-value < 0.01)
398 after TGF-β stimulation **(Figure 7C, D)**.

399

# DISCUSSION

While the role of the centrosome in the control of the mitotic cycle has been very well studied, little is known about its structure and functions in other contexts (Doxsey et al., 2005; Bettencourt-Dias and Glover, 2007; Conduit et al., 2015). The study of different mutated centrosomal proteins and their impact on processes of the primary cilium, such as ciliogenesis, endocytosis or the signalling of various pathways such as WNT, SHh or TGF-β, has however been enlightening (Kobayashi and Dynlacht, 2011; Collin et al., 2012; Hehnly et al., 2012; Leitch et al., 2014; Mönnich et al., 2018; Gonçalves et al., 2021). Despite all this, many of the regulatory aspects of how centrosomal proteins coordinate these processes remain unknown.

The TGF-β signalling is one of the main pathways regulated through the primary cilium (Clement et al., 2013). It is involved in normal development in mammals and influences other pathways by cross-signalling such as p53, MAPKs or PI3K/AKT (Rahimi and Leof, 2007; Patel et al., 2019; Finnson et al., 2020). For this reason, it is timely to determine the role of different ciliary and basal body genes, such as *ALMS1*, in their regulation.

Thus, we further explored the previously described association between ALMS1 deficiency and alterations in TGF-β-mediated signal transduction (Álvarez-Satta et al., 2021; Bea-Mascato et al., 2022). We performed gene expression profiling by RNA-seq and LFQ-proteomics in an ALMS1KO hTERT-BJ-5ta cell line stimulated with TGF-β1. This cellular model was previously generated and characterised in our lab (Bea-Mascato et al., 2022). We found that the lack of ALMS1 generates an inhibited gene expression profile after TGF-β1 stimulation, both in the transcriptome and proteome **(Figure 2A; 4A)**. This gene expression profile is consistent with our previously described proteomic results in HeLa and with the basal gene expression profile described in patient fibroblasts (Zulato et al., 2011; Bea-Mascato et al., 2022). This means that the lack of ALMS1 is likely to have an inhibitory impact on most of the processes controlled downstream of this gene, such as mitosis, cell migration or receptor recycling. (Zulato et al., 2011; Leitch et al., 2014; Shenje et al., 2014; Bea-Mascato et al., 2022).

The ORA of transcriptome revealed alterations in the TGF-β signalling pathway and other tangentially regulated pathways such as mTOR, EGFR or p53 and processes such as ECM

430 regulation or EMT **(Figure 2B, C)**. The existence of this cross-signalling is known,
431 however, this is the first time that the impact of ALMS1 depletion on it has been shown,
432 which could open up new avenues of treatment for ALMS patients. (Kato et al., 2009;
433 Hamidi et al., 2017; Patel et al., 2019). On the other hand, It was previously established,
434 that ALMS1 depletion led to aberrant expression of several TGF-β1-induced EMT
435 markers in HeLa and hTERT-BJ-5ta cells (Bea-Mascato et al., 2022). However, these
436 results further establish the connection between ALMS1 depletion and EMT alterations.
437 EMT inhibition supports the poor migration capacity of cells lacking ALMS1 which may
438 be due to cytoskeleton collapse, another event described in cells lacking ALMS1 (Zulato
439 et al., 2011; Collin et al., 2012; Bea-Mascato et al., 2022).

440 Downstream activation of the TGF-β pathway can follow *via* the canonical pathway,
441 dependent on SMADs (SMAD2 and SMAD3), or non-canonical, which encompasses a
442 plethora of pathways such as MAPKs, ERKs, p53, or PI3K/AKT (Finnson et al., 2020). For
443 this reason, alterations in cross-signalling pathways such as mTORC1, EGFR1 or p53
444 detected in the transcriptome show that alterations in TGF-β are mainly related to the
445 non-canonical part of this pathway **(Figure 2C)** (Patel et al., 2019; Finnson et al., 2020).

446 Our proteomic analysis revealed proteins involved in lipid metabolism and cytoplasmic
447 organelles such as the endoplasmic reticulum, mitochondria, or lysosomes **(Figure 4B,**
448 **C)**. We have previously described that ALMS1 depletion does impact cell viability due to
449 changes in mitochondrial reduction capacity (Bea-Mascato et al., 2022). However, it
450 appears to affect mitochondrial β-oxidation of fatty acids **(Figure 4C)**. This could connect
451 the absence of ALMS1 to oxidative metabolism disorders (Liu and Desai, 2015). In
452 addition, alterations in cytoplasmic organelles, such as the endoplasmic reticulum and
453 lysosomes, could be related to alterations in endocytosis, receptor recycling or
454 autophagy. ALMS1 absence has been linked to alterations in transferrin (TfR), NOTCH
455 and NKCC2 receptor recycling, but its role in TGF-β receptor recycling or autophagy has
456 not yet been established (Collin et al., 2012; Leitch et al., 2014; Jaykumar et al., 2018;
457 Yang et al., 2020).

458 Indeed, after applying a redundancy reduction analysis of enriched pathways, we found
459 that ALMS1 regulates two main clusters in the transcriptome and proteome; processes
460 related to the regulation of the ECM and processes related to lipid metabolism such as

461 β-oxidation of fatty acids **(Figure 3; 5)**. It has already been described that deletion of
462 ALMS1 leads to overexpression of several ECM components in fibroblasts from ALMS
463 patients. For this reason, understanding these alterations is key to determining the
464 pathophysiology of fibrosis in ALMS (Zulato et al., 2011). On the other hand, the
465 metabolic alterations observed in ALMS could have their origin in processes such as β-
466 oxidation of fatty acids (Romano et al., 2008; Huang-Doran and Semple, 2010; Favaretto
467 et al., 2014; Geberhiwot et al., 2021).

468 The list of common differentially expressed genes between the transcriptome and
469 proteome supports the above findings, indicating that ALMS1 depletion affects EMT,
470 endoplasmic reticulum, Syndecan-1 and BDNF signalling pathways and lipid metabolism
471 pathways such as β-oxidation of fatty acids **(Figure 6D, E)** (Kasza et al., 2014). By studying
472 this list of genes by redundancy reduction analysis, we saw the existence of a link
473 between ALMS1 depletion and eicosanoid metabolism in addition to the processes
474 mentioned above **(Figure 6F)**. Alterations related to the ECM are undoubtedly key to the
475 appearance of fibrosis in these patients; however, alterations in the β-oxidation of fatty
476 acids, beyond their link to obesity, may contribute to the appearance of fibrotic tissue
477 due to lipid deposits (Serra et al., 2013; Kang et al., 2014). This suggest that the
478 metabolic disorder in patients with ALMS is involved in the progressive development of
479 fibrosis in various organs such as the kidneys and liver (Bettini et al., 2021).

480 Regarding the deregulation of the PI3K/AKT, we can relate the over-activation of AKT
481 **(Figure 7A, B)** with the inhibition of the p53 pathway **(Figure 1C)** (Gottlieb et al., 2002;
482 Abraham and O'Neill, 2014). This is supported by the decrease in the expression of the
483 *PTEN* gene, which could explain an over-phosphorylation of the cell membrane and an
484 accumulation of PIP3 leading to the over-activation of AKT **(Figure 7C, D)** (Álvarez-Garcia
485 et al., 2019). To our knowledge, this is the first study to explore how *ALMS1* affects cross-
486 signalling between AKT and the TGF-β pathway. Other studies have been carried out to
487 try to understand the role of *ALMS1* in regulating the insulin mediated AKT pathway.
488 The involvement of AKT has not yet been clearly established in ALMS, while some studies
489 in pre-adipocytes have not detected any differences in AKT activation, other studies in
490 mice have shown that AKT is over-activated in some tissues and it is inhibited in others,
491 when *ALMS1* is depleted (Huang-Doran and Semple, 2010; Favaretto et al., 2014;

492 Geberhiwot et al., 2021). AKT regulation is tissue specific, it has 3 distinct isoforms and
493 each has multiple phosphorylation sites (Liao and Hung, 2010). This could be an
494 explanation for the disparity of the data present in the bibliography.

495 The over-activation of the AKT pathway could be the link between alterations at the
496 metabolic level and alterations related to the ECM. The inhibition of p53 would be
497 caused by this over-activation through MDM2, affecting the PTEN-p53-AKT-MDM2 loop
498 (Gottlieb et al., 2002; Abraham and O'Neill, 2014). This hypothesis would be supported
499 by the resistance to apoptosis in *ALMS1*-depleted cells (Zulato et al., 2011; Bea-Mascato
500 et al., 2022).

# 501 CONCLUSION

502 In conclusion, the lack of *ALMS1* gene expression alters the TGF-β pathway in the
503 knockout cell model. It also seems to compromise the signalling of other tangential
504 pathways such as PI3K/AKT or p53. These signalling alterations appear to affect diverse
505 metabolic processes involving the mitochondrial, endoplasmic reticulum and lysosomes
506 and various lipid-mediated signalling pathways. The alterations are mainly clustered into
507 processes affecting the regulation of the ECM and the β-oxidation of fatty acids, which
508 we confirmed in both the transcriptome and proteome. Finally, *ALMS1* depletion led to
509 over-activation of the AKT protein in BJ-5ta cells and inhibition of the PTEN protein in
510 HeLa cells.

511 **Author Contributions:** BB-M, DV designed the study. BB-M performed the experiments,
512 analysed the data, interpreted the results, created the figures, and drafted the first
513 manuscript. EG-C, YS-C and SC helped with RNA-seq analysis and data integration. DV
514 supervised the study and performed funding acquisition. All authors provided
515 comments and corrections to the manuscript and gave their approval for publication.

516 **Funding:** This work was funded by Instituto de Salud Carlos III de Madrid FIS project
517 PI15/00049 and PI19/00332, Xunta de Galicia (Centro de Investigación de Galicia CINBIO
518 2019-2022) Ref. ED431G-2019/06, Consolidación e estructuración de unidades de
519 investigación competitivas e outras accións de fomento (ED431C-2018/54). Brais Bea-
520 Mascato (FPU17/01567) was supported by graduate studentship awards (FPU

predoctoral fellowship) from the Spanish Ministry of Education, Culture and Sports. We thank the NIHR GOSH BRC for its support (to YE S-C and SC).

**Informed Consent Statement:** Not Apply.

**Data Availability Statement:** Data are available via Gene Expression Omnibus (GEO) with the identifier GSE209844 and ProteomeXchange with the identifier PXD035708.

**Code Availability Statement:** The code used in this study can be accessed at the GitHub address "https://github.com/BreisOne/multiomic_pipeline".

**Acknowledgements:** We sincerely thank the Proteomics and Genomics services from "Centro de Apoyo Científico-Tecnológico a la Investigación" (CACTI) of University of Vigo and its specialists Paula Álvarez Chaver, Ángel Sebastián Comesaña, Verónica Outeiriño and Manuel Marcos for their guidance and advise. We also thank Mercedes Peleteiro Olmedo from "Centro de Investigacións Biomédicas" (CINBIO) from University of Vigo for the flow cytometry service.

**Conflicts of Interest:** The authors declare no conflict of interest. The funders had no role in the design of the study; in the collection, analyses, or interpretation of data; in the writing of the manuscript, or in the decision to publish the results.

538 # REFERENCES


539 Abraham, A. G., and O'Neill, E. (2014). PI3K/Akt-mediated regulation of p53 in cancer.
540 *Biochem. Soc. Trans.* 42, 798–803. doi: 10.1042/BST20140070.

541 Álvarez-Garcia, V., Tawil, Y., Wise, H. M., and Leslie, N. R. (2019). Mechanisms of PTEN
542 loss in cancer: It's all about diversity. *Semin. Cancer Biol.* 59, 66–79. doi:
543 10.1016/J.SEMCANCER.2019.02.001.

544 Álvarez-Satta, M., Lago-Docampo, M., Bea-Mascato, B., Solarat, C., Castro-Sánchez, S.,
545 Christensen, S. T., et al. (2021). ALMS1 Regulates TGF-β Signaling and Morphology
546 of Primary Cilia. *Front. Cell Dev. Biol.* 9, 112. doi: 10.3389/fcell.2021.623829.

547 Anders, S., Pyl, P. T., and Huber, W. (2015). HTSeq—a Python framework to work with
548 high-throughput sequencing data. *Bioinformatics* 31, 166–169. doi:
549 10.1093/bioinformatics/btu638.

550 Anvarian, Z., Mykytyn, K., Mukhopadhyay, S., Pedersen, L. B., and Christensen, S. T.
551 (2019). Cellular signalling by primary cilia in development, organ function and
552 disease. *Nat. Rev. Nephrol.* 15, 199–219. doi: 10.1038/s41581-019-0116-9.

553 Barrett, T., Wilhite, S. E., Ledoux, P., Evangelista, C., Kim, I. F., Tomashevsky, M., et al.
554 (2013). NCBI GEO: archive for functional genomics data sets—update. *Nucleic Acids*
555 *Res.* 41, D991. doi: 10.1093/NAR/GKS1193.

556 Bea-Mascato, B., Giudice, G., Pinheiro-de-Sousa, I., Solarat, C., Petsalaki, E., and
557 Valverde, D. (2023). Phosphoproteomic profiling highlights CDC42 and CDK2 as key
558 players in the regulation of the TGF-β pathway in ALMS1 and BBS1 knockout
559 models. *bioRxiv*, 2022.11.04.514246. doi: 10.1101/2022.11.04.514246.

560 Bea-Mascato, B., Neira-Goyanes, E., Iglesias-Rodríguez, A., and Valverde, D. (2022).
561 Depletion of ALMS1 affects TGF-β signalling pathway and downstream processes
562 such as cell migration and adhesion capacity. *Front. Mol. Biosci.* 9, 1085. doi:
563 10.3389/fmolb.2022.992313.

564 Bettencourt-Dias, M., and Glover, D. M. (2007). Centrosome biogenesis and function:
565 centrosomics brings new understanding. *Nat. Rev. Mol. Cell Biol.* 8, 451–463. doi:

566 10.1038/NRM2180.

567 Bettini, S., Bombonato, G., Dassie, F., Favaretto, F., Piffer, L., Bizzotto, P., et al. (2021).
568 Liver Fibrosis and Steatosis in Alström Syndrome: A Genetic Model for Metabolic
569 Syndrome. *Diagnostics 2021, Vol. 11, Page 797* 11, 797. doi:
570 10.3390/DIAGNOSTICS11050797.

571 Chen, J.-H., Geberhiwot, T., Barrett, T. G., Paisey, R., and Semple, R. K. (2017). Refining
572 genotype-phenotype correlation in Alström syndrome through study of primary
573 human fibroblasts. *Mol. Genet. genomic Med.* 5, 390–404. doi: 10.1002/mgg3.296.

574 Christensen, S. T., Morthorst, S. K., Mogensen, J. B., and Pedersen, L. B. (2017). Primary
575 Cilia and Coordination of Receptor Tyrosine Kinase (RTK) and Transforming Growth
576 Factor β (TGF-β) Signaling. *Cold Spring Harb. Perspect. Biol.* 9, a028167. doi:
577 10.1101/CSHPERSPECT.A028167.

578 Clement, C. A., Ajbro, K. D., Koefoed, K., Vestergaard, M. L., Veland, I. R., Henriques de
579 Jesus, M. P. R., et al. (2013). TGF-β signaling is associated with endocytosis at the
580 pocket region of the primary cilium. *Cell Rep.* 3, 1806–14. doi:
581 10.1016/j.celrep.2013.05.020.

582 Collin, G. B., Cyr, E., Bronson, R., Marshall, J. D., Gifford, E. J., Hicks, W., et al. (2005).
583 Alms1-disrupted mice recapitulate human Alström syndrome. *Hum. Mol. Genet.*
584 14, 2323–2333. doi: 10.1093/hmg/ddi235.

585 Collin, G. B., Marshall, J. D., Ikeda, A., So, W. V., Russell-Eggitt, I., Maffei, P., et al. (2002).
586 Mutations in ALMS1 cause obesity, type 2 diabetes and neurosensory degeneration
587 in Alström syndrome. *Nat. Genet.* 31, 74–8. doi: 10.1038/ng867.

588 Collin, G. B., Marshall, J. D., King, B. L., Milan, G., Maffei, P., Jagger, D. J., et al. (2012).
589 The Alström syndrome protein, ALMS1, interacts with α-actinin and components of
590 the endosome recycling pathway. *PLoS One* 7, e37925–e37925. doi:
591 10.1371/journal.pone.0037925.

592 Conduit, P. T., Wainman, A., and Raff, J. W. (2015). Centrosome function and assembly
593 in animal cells. *Nat. Rev. Mol. Cell Biol.* 16, 611–624. doi: 10.1038/NRM4062.

594 Dobin, A., Davis, C. A., Schlesinger, F., Drenkow, J., Zaleski, C., Jha, S., et al. (2013). STAR:
595 ultrafast universal RNA-seq aligner. *Bioinformatics* 29, 15–21. doi:
596 10.1093/bioinformatics/bts635.

597 Doxsey, S., Zimmerman, W., and Mikule, K. (2005). Centrosome control of the cell cycle.
598 *Trends Cell Biol.* 15, 303–311. doi: 10.1016/J.TCB.2005.04.008.

599 Ewels, P., Magnusson, M., Lundin, S., and Käller, M. (2016). MultiQC: summarize analysis
600 results for multiple tools and samples in a single report. *Bioinformatics* 32, 3047–
601 3048. doi: 10.1093/BIOINFORMATICS/BTW354.

602 Favaretto, F., Milan, G., Collin, G. B., Marshall, J. D., Stasi, F., Maffei, P., et al. (2014).
603 GLUT4 Defects in Adipose Tissue Are Early Signs of Metabolic Alterations in
604 Alms1GT/GT, a Mouse Model for Obesity and Insulin Resistance. *PLoS One* 9,
605 e109540. doi: 10.1371/JOURNAL.PONE.0109540.

606 Finnson, K. W., Almadani, Y., and Philip, A. (2020). Non-canonical (non-SMAD2/3) TGF-β
607 signaling in fibrosis: Mechanisms and targets. *Semin. Cell Dev. Biol.* 101, 115–122.
608 doi: 10.1016/J.SEMCDB.2019.11.013.

609 Geberhiwot, T., Baig, S., Obringer, C., Girard, D., Dawson, C., Manolopoulos, K., et al.
610 (2021). Relative Adipose Tissue Failure in Alström Syndrome Drives Obesity-
611 Induced Insulin Resistance. *Diabetes* 70, 364–376. doi: 10.2337/DB20-0647.

612 Gonçalves, A. B., Hasselbalch, S. K., Joensen, B. B., Patzke, S., Martens, P., Ohlsen, S. K.,
613 et al. (2021). CEP78 functions downstream of CEP350 to control biogenesis of
614 primary cilia by negatively regulating CP110 levels. *Elife* 10. doi:
615 10.7554/ELIFE.63731.

616 Gottlieb, T. M., Martinez Leal, J. F., Seger, R., Taya, Y., and Oren, M. (2002). Cross-talk
617 between Akt, p53 and Mdm2: possible implications for the regulation of apoptosis.
618 *Oncogene 2002 218* 21, 1299–1303. doi: 10.1038/sj.onc.1205181.

619 Graser, S., Stierhof, Y.-D., Lavoie, S. B., Gassner, O. S., Lamla, S., Le Clech, M., et al.
620 (2007). Cep164, a novel centriole appendage protein required for primary cilium
621 formation. *J. Cell Biol.* 179, 321–330. doi: 10.1083/jcb.200707181.

622 Hamidi, A., Song, J., Thakur, N., Itoh, S., Marcusson, A., Bergh, A., et al. (2017). TGF-β
623 promotes PI3K-AKT signaling and prostate cancer cell migration through the TRAF6-
624 mediated ubiquitylation of p85α. *Sci. Signal.* 10. doi: 10.1126/SCISIGNAL.AAL4186.

625 Hearn, T. (2018). ALMS1 and Alström syndrome: a recessive form of metabolic,
626 neurosensory and cardiac deficits. *J. Mol. Med.* doi: 10.1007/s00109-018-1714-x.

627 Hearn, T., Spalluto, C., Phillips, V. J., Renforth, G. L., Copin, N., Hanley, N. A., et al. (2005).
628 Subcellular Localization of ALMS1 Supports Involvement of Centrosome and Basal
629 Body Dysfunction in the Pathogenesis of Obesity, Insulin Resistance, and Type 2
630 Diabetes. *Diabetes* 54, 1581 LP – 1587. doi: 10.2337/diabetes.54.5.1581.

631 Hehnly, H., Chen, C. T., Powers, C. M., Liu, H. L., and Doxsey, S. (2012). The Centrosome
632 Regulates the Rab11- Dependent Recycling Endosome Pathway at Appendages of
633 the Mother Centriole. *Curr. Biol.* 22, 1944–1950. doi: 10.1016/J.CUB.2012.08.022.

634 Hoxhaj, G., and Manning, B. D. (2019). The PI3K–AKT network at the interface of
635 oncogenic signalling and cancer metabolism. *Nat. Rev. Cancer 2019 202* 20, 74–88.
636 doi: 10.1038/s41568-019-0216-7.

637 Huang-Doran, I., and Semple, R. K. (2010). Knockdown of the Alström syndrome-
638 associated gene Alms1 in 3T3-L1 preadipocytes impairs adipogenesis but has no
639 effect on cell-autonomous insulin action. *Int. J. Obes. 2010 3410* 34, 1554–1558.
640 doi: 10.1038/ijo.2010.92.

641 Ishikawa, H., and Marshall, W. F. (2011). Ciliogenesis: building the cell's antenna. *Nat.*
642 *Rev. Mol. Cell Biol.* 12, 222–234. doi: 10.1038/NRM3085.

643 Jagger, D., Collin, G., Kelly, J., Towers, E., Nevill, G., Longo-Guess, C., et al. (2011). Alström
644 Syndrome protein ALMS1 localizes to basal bodies of cochlear hair cells and
645 regulates cilium-dependent planar cell polarity. *Hum. Mol. Genet.* 20, 466–481. doi:
646 10.1093/hmg/ddq493.

647 Jaykumar, A. B., Caceres, P. S., King-Medina, K. N., Liao, T.-D., Datta, I., Maskey, D., et al.
648 (2018). Role of Alström syndrome 1 in the regulation of blood pressure and renal
649 function. *JCI insight* 3, e95076. doi: 10.1172/jci.insight.95076.

650 Kang, H. M., Ahn, S. H., Choi, P., Ko, Y. A., Han, S. H., Chinga, F., et al. (2014). Defective
651 fatty acid oxidation in renal tubular epithelial cells has a key role in kidney fibrosis
652 development. *Nat. Med. 2014 211* 21, 37–46. doi: 10.1038/nm.3762.

653 Kasza, I., Suh, Y., Wollny, D., Clark, R. J., Roopra, A., Colman, R. J., et al. (2014). Syndecan-
654 1 Is Required to Maintain Intradermal Fat and Prevent Cold Stress. *PLOS Genet.* 10,
655 e1004514. doi: 10.1371/JOURNAL.PGEN.1004514.

656 Kato, M., Putta, S., Wang, M., Yuan, H., Lanting, L., Nair, I., et al. (2009). TGF-beta
657 activates Akt kinase through a microRNA-dependent amplifying circuit targeting
658 PTEN. *Nat. Cell Biol.* 11, 881–889. doi: 10.1038/NCB1897.

659 Knorz, V. J., Spalluto, C., Lessard, M., Purvis, T. L., Adigun, F. F., Collin, G. B., et al. (2010).
660 Centriolar association of ALMS1 and likely centrosomal functions of the ALMS
661 motif-containing proteins C10orf90 and KIAA1731. *Mol. Biol. Cell* 21, 3617–29. doi:
662 10.1091/mbc.E10-03-0246.

663 Kobayashi, T., and Dynlacht, B. D. (2011). Regulating the transition from centriole to
664 basal body. *J. Cell Biol.* 193, 435–444. doi: 10.1083/JCB.201101005.

665 Kuleshov, M. V., Jones, M. R., Rouillard, A. D., Fernandez, N. F., Duan, Q., Wang, Z., et al.
666 (2016). Enrichr: a comprehensive gene set enrichment analysis web server 2016
667 update. *Nucleic Acids Res.* 44, W90. doi: 10.1093/NAR/GKW377.

668 Leitch, C. C., Lodh, S., Prieto-Echagüe, V., Badano, J. L., and Zaghloul, N. A. (2014). Basal
669 body proteins regulate Notch signaling through endosomal trafficking. *J. Cell Sci.*
670 127, 2407–19. doi: 10.1242/jcs.130344.

671 Li, G., Vega, R., Nelms, K., Gekakis, N., Goodnow, C., McNamara, P., et al. (2007). A role
672 for Alström syndrome protein, alms1, in kidney ciliogenesis and cellular quiescence.
673 *PLoS Genet.* 3, e8. doi: 10.1371/journal.pgen.0030008.

674 Liao, Y., and Hung, M. C. (2010). Physiological regulation of Akt activity and stability. *Am.*
675 *J. Transl. Res.* 2, 19. Available at: /pmc/articles/PMC2826820/ [Accessed August 22,
676 2022].

677 Liu, R. M., and Desai, L. P. (2015). Reciprocal regulation of TGF-β and reactive oxygen

678 species: A perverse cycle for fibrosis. *Redox Biol.* 6, 565. doi:
679 10.1016/J.REDOX.2015.09.009.

680 Love, M. I., Huber, W., and Anders, S. (2014). Moderated estimation of fold change and
681 dispersion for RNA-seq data with DESeq2. *Genome Biol.* 15, 550. doi:
682 10.1186/s13059-014-0550-8.

683 May-Simera, H. L., Wan, Q., Jha, B. S., Hartford, J., Khristov, V., Dejene, R., et al. (2018).
684 Primary Cilium-Mediated Retinal Pigment Epithelium Maturation Is Disrupted in
685 Ciliopathy Patient Cells. *Cell Rep.* 22, 189–205. doi: 10.1016/j.celrep.2017.12.038.

686 May-Simera, H., Nagel-Wolfrum, K., and Wolfrum, U. (2017). Cilia - The sensory
687 antennae in the eye. *Prog. Retin. Eye Res.* 60, 144–180. doi:
688 10.1016/J.PRETEYERES.2017.05.001.

689 Merico, D., Isserlin, R., Stueker, O., Emili, A., and Bader, G. D. (2010). Enrichment Map:
690 A Network-Based Method for Gene-Set Enrichment Visualization and
691 Interpretation. *PLoS One* 5, e13984. doi: 10.1371/JOURNAL.PONE.0013984.

692 Mönnich, M., Borgeskov, L., Breslin, L., Jakobsen, L., Rogowski, M., Doganli, C., et al.
693 (2018). CEP128 Localizes to the Subdistal Appendages of the Mother Centriole and
694 Regulates TGF-β/BMP Signaling at the Primary Cilium. *Cell Rep.* 22, 2584–2592. doi:
695 10.1016/J.CELREP.2018.02.043.

696 Pala, R., Alomari, N., and Nauli, S. M. (2017). Primary Cilium-Dependent Signaling
697 Mechanisms. *Int. J. Mol. Sci.* 18. doi: 10.3390/IJMS18112272.

698 Patel, S., Tang, J., Overstreet, J. M., Anorga, S., Lian, F., Arnouk, A., et al. (2019). Rac-
699 GTPase promotes fibrotic TGF-β1 signaling and chronic kidney disease via EGFR,
700 p53, and Hippo/YAP/TAZ pathways. *FASEB J.* 33, 9797–9810. doi:
701 10.1096/FJ.201802489RR.

702 Perez-Riverol, Y., Csordas, A., Bai, J., Bernal-Llinares, M., Hewapathirana, S., Kundu, D.
703 J., et al. (2019). The PRIDE database and related tools and resources in 2019:
704 improving support for quantification data. *Nucleic Acids Res.* 47, D442–D450. doi:
705 10.1093/nar/gky1106.

706 Rahimi, R. A., and Leof, E. B. (2007). TGF-β signaling: A tale of two responses. *J. Cell.*
707 *Biochem.* 102, 593–608. doi: 10.1002/JCB.21501.

708 Reimand, J., Isserlin, R., Voisin, V., Kucera, M., Tannus-Lopes, C., Rostamianfar, A., et al.
709 (2019). Pathway enrichment analysis and visualization of omics data using
710 g:Profiler, GSEA, Cytoscape and EnrichmentMap. *Nat. Protoc.* 14, 482–517. doi:
711 10.1038/S41596-018-0103-9.

712 Ritchie, M. E., Phipson, B., Wu, D., Hu, Y., Law, C. W., Shi, W., et al. (2015). limma powers
713 differential expression analyses for RNA-sequencing and microarray studies.
714 *Nucleic Acids Res.* 43, e47–e47. doi: 10.1093/NAR/GKV007.

715 Romano, S., Milan, G., Veronese, C., Collin, G. B., Marshall, J. D., Centobene, C., et al.
716 (2008). Regulation of Alström syndrome gene expression during adipogenesis and
717 its relationship with fat cell insulin sensitivity. *Int. J. Mol. Med.* 21, 731–736. doi:
718 10.3892/IJMM.21.6.731/HTML.

719 Schindelin, J., Arganda-Carreras, I., Frise, E., Kaynig, V., Longair, M., Pietzsch, T., et al.
720 (2012). Fiji: an open-source platform for biological-image analysis. *Nat. Methods*
721 *2012 97* 9, 676–682. doi: 10.1038/nmeth.2019.

722 Serra, D., Mera, P., Malandrino, M. I., Mir, J. F., and Herrero, L. (2013). Mitochondrial
723 Fatty Acid Oxidation in Obesity. *https://home.liebertpub.com/ars* 19, 269–284. doi:
724 10.1089/ARS.2012.4875.

725 Shenje, L. T., Andersen, P., Halushka, M. K., Lui, C., Fernandez, L., Collin, G. B., et al.
726 (2014). Mutations in Alström protein impair terminal differentiation of
727 cardiomyocytes. *Nat. Commun.* 5, 3416. doi: 10.1038/ncomms4416.

728 Varet, H., Brillet-Guéguen, L., Coppée, J.-Y., and Dillies, M.-A. (2016). SARTools: A
729 DESeq2- and EdgeR-Based R Pipeline for Comprehensive Differential Analysis of
730 RNA-Seq Data. *PLoS One* 11, e0157022. Available at:
731 https://doi.org/10.1371/journal.pone.0157022.

732 Wickham, H. (2016). *ggplot2: Elegant Graphics for Data Analysis*. Springer-Verlag New
733 York Available at: https://ggplot2.tidyverse.org.

734 Xu, W., Yang, Z., and Lu, N. (2015). A new role for the PI3K/Akt signaling pathway in the
735 epithelial-mesenchymal transition.
736 *http://dx.doi.org/10.1080/19336918.2015.1016686* 9, 317–324. doi:
737 10.1080/19336918.2015.1016686.

738 Yang, C., Chen, X. C., Li, Z. H., Wu, H. L., Jing, K. P., Huang, X. R., et al. (2020). SMAD3
739 promotes autophagy dysregulation by triggering lysosome depletion in tubular
740 epithelial cells in diabetic nephropathy.
741 *https://doi.org/10.1080/15548627.2020.1824694* 17, 2325–2344. doi:
742 10.1080/15548627.2020.1824694.

743 Yu, J. S. L., and Cui, W. (2016). Proliferation, survival and metabolism: the role of
744 PI3K/AKT/mTOR signalling in pluripotency and cell fate determination.
745 *Development* 143, 3050–3060. doi: 10.1242/DEV.137075.

746 Zhang, X., Smits, A. H., van Tilburg, G. B., Ovaa, H., Huber, W., and Vermeulen, M. (2018).
747 Proteome-wide identification of ubiquitin interactions using UbIA-MS. *Nat. Protoc.*
748 13, 530–550. doi: 10.1038/nprot.2017.147.

749 Zulato, E., Favaretto, F., Veronese, C., Campanaro, S., Marshall, J. D., Romano, S., et al.
750 (2011). ALMS1-deficient fibroblasts over-express extra-cellular matrix components,
751 display cell cycle delay and are resistant to apoptosis. *PLoS One* 6, e19081–e19081.
752 doi: 10.1371/journal.pone.0019081.

753